Revision 3

Word count: 5595

Illitization of smectite influenced by chemical weathering and its potential control of anatase formation in altered volcanic ashes

Chen Liu[1#], Qian Fang[1#], Hanlie Hong[1*], Qian Song[1], Kaipeng Ji[1], Nina Gong[1,2], Xibing Shen[1,3], Thomas J. Algeo[1,4,5]

[1] State Key Laboratory of Biogeology and Environmental Geology, School of Earth Sciences, China University of Geosciences, Wuhan 430074, China

[2] Jewelry Institute of Guangzhou Panyu Polytechnic, Guangzhou 511487, Guangdong, China

[3] School of Resources and Environment, Beibu Gulf University, Qinzhou, Guangxi 535011, China

[4] State Key Laboratory of Geological Processes and Mineral Resources, China University of Geosciences, Wuhan 430074, China

[5] Department of Geosciences, University of Cincinnati, OH 45221-0013, USA

[#]These authors contributed equally to this paper.

*Corresponding author. E-mail addresses: honghanlie@cug.edu.cn (H. Hong)

Abstract

Illitization of smectite in sedimentary systems, a process akin to 'reverse weathering', is a diagenetic process that has significant implications for sediment paragenesis and hydrocarbon exploration. However, the potential influence of chemical weathering on the illitization of smectite, and its possible control of the neogenesis of titanium (Ti)-oxides remain unclear. Altered volcanic tephra layers (i.e., K-bentonites) characterized by an interstratified illite-smectite (I-S) clay mineralogy serve as an excellent medium to investigate the illitization of smectite. In this study, we first investigated the fine structure of clay minerals and in-situ nano-mineralogy of

Ti-bearing minerals from altered volcanic ashes and then undertook a meta-analysis of geochemical compositional data for bentonites spanning a wide range of ages and depositional environments globally. We found that Ti mainly occurs as discrete micron-scale magmatic srilankite and nanoscale authigenic anatase crystals. During the weathering process, the magmatic srilankite partly dissolved under acidic conditions, resulting in a local buildup of Ti in porewaters. The I-S displays a platy habit and curved edges and is found closely associated with anatase crystals under TEM. Our compilation results combined with microscopic evidence suggest that chemical weathering may potentially promote the illitization reaction by changing the chemical composition of the fluids through increased terrestrial inputs and by creating larger pore spaces through decomposition of weatherable components. Positive correlations between K and Ti are especially common in (K-)bentonites that are dominated by I-S, suggesting that I-S can adsorb Ti during the weathering process and provide a suitable site for the nucleation of anatase. Our study highlights the role of chemical weathering in the illitization of smectite and their combined effect on the formation of Ti-oxides.

Keywords: nanoscale; meta-analysis; illite; Ti-oxides; diagenesis; mixed-layer;

1. Introduction

In sedimentary and hydrothermal systems, the illitization of smectite forms interstratified illite-smectite (I-S) phases, with the extent of illitization thought to be controlled mainly by diagenetic temperature and fluid composition (Schroeder and Nagasawa, 1992; Huff, 2016; Wilson et al., 2016a, b). The illitization of smectite is akin to 'reverse weathering' in that it requires K^+ incorporation into a smectite precursor (Isson and Planavsky, 2018; Aubineau et al., 2019). The proportion of illite in I-S has been used as a tracer for reconstruction of the evolutionary history of sedimentary basins and hydrothermal systems (Cuadros and Altaner, 1998; Yuan et al., 2013; Bozkaya et al., 2016; Wilson et al., 2016a, b). However, chemical weathering, a widespread process occurring at the water-rock interface, can alter rock compositions and the chemical stability of minerals. Chemical weathering of volcanic

ashes (i.e., (K-)bentonites) is initiated immediately after their deposition and encompasses the entire range of alteration processes operating from the surface to near-surface environment. These processes may exert influences on the illitization of smectite, shaping the type of information preserved by I-S, especially concerning the burial and hydrocarbon accumulation history of a sedimentary basin. The altered volcanic ashes are often linked to large explosive volcanic eruptions that happened in geological history (Huff, 2016). Previous studies have demonstrated that (K-)bentonites (i.e., altered volcanic ash beds) are useful for stratigraphic correlation and for interpreting Earth's geodynamic evolution (Huff, 2016; Hong et al., 2017). One of the most important characteristics of (K-)bentonites is their clay mineralogy, which is commonly dominated by I-S.

Ti-oxides are another important component of (K-)bentonites, yet their origin is often unclear. The sorptive behavior of I-S phases produced by the illitization process creates the potential for interaction with Ti ions or newly formed authigenic TiO_2 particles, thereby influencing the migration and sequestration of Ti. These influences may contribute, in turn, to the preservation of Ti, rendering its utility as an inert element used in the discrimination of magma source and sediment provenance problematic. However, to the best of our knowledge, such influences have never been reported, and our understanding of related processes remains poor. Deciphering the origin of authigenic Ti-oxides and the role of I-S in their formation is essential for understanding Ti fluxes in natural environments. Although extensive studies have been published regarding the formation of I-S in (K-)bentonites (Christidis, 1998; Cornu et al., 1999; Xu et al., 2017; Zhu et al., 2022), the roles of chemical weathering in the illitization of smectite and the migratory behavior of Ti have rarely been examined (Hong et al., 2020).

In this study, we investigated the fine structure of clay minerals and the nano-mineralogical characteristics of Ti-bearing minerals in altered volcanic ashes from a marine Permian-Triassic boundary (PTB) succession in South China. We supplemented this dataset by compiling geochemical data from published studies encompassing 384 (K-)bentonite samples with a global distribution. This study aims

to uncover the origin of Ti-oxides in (K-)bentonite, the potential influence of chemical weathering on the illitization of smectite, and the joint influence of chemical weathering and smectite illitization on the formation of Ti-oxides in (K-)bentonite.

2. Materials and methods

2.1. Geological setting

The Xiakou section (31°6'52.75"N, 110°48'12.87"E) is located in northwestern Yichang City and outcrops along a highway from Yichang to Xingshan County (Fig. 1). It is situated in the northern part of the Yangtze Platform, near the Huangling Uplift. The region is characterized by north-south trending structures and a shallow-marine sedimentary environment during the Permian-Triassic transition (Wang, 1998). The lower part of the section consists mainly of dark-gray mudstone with limestone and argillaceous limestone interbeds of the Upper Permian Dalong Formation, and its upper part of limestone, mudstone, and marlstone of the Lower Triassic Daye Formation. Six altered volcanic ash samples (Beds L255, L260, L264, L266, L271, and L277) were collected from near the Permian-Triassic boundary, ranging from 2 to 10 cm in thickness (Fig. 2).

2.2. X-ray diffractometry (XRD)

The altered volcanic ash samples were first dried in an oven at 40°C and then ground to fine powder with a particle size < 74 μm. For bulk samples, random powder mounts in a sample holder were prepared using a back-press technique in order to avoid preferential orientation of minerals. For clay fractions (< 2 μm), the volcanic ash samples were initially treated with 0.025 mol/L HCl to eliminate carbonates, followed by the addition of 5 mL of 30% H_2O_2 to remove organic matter. After the reactions were completed, clay fractions were isolated using the sedimentation method outlined by Jackson (1978). The oriented clay samples were prepared by pipetting a purified clay suspension onto a glass slide that was allowed to air-dry at room temperature. Both air-dried (AD) and ethylene-glycol-saturated (EG) mounts of clay fractions were prepared to identify mixed-layer clay minerals. The XRD patterns were recorded using a X'Pert PRO DY2198 diffractometer at the China University of

Geosciences (Wuhan), operated at 35 kV and 30 mA with slit settings of 1° for the divergence and anti-scatter slits and 0.3 mm for the receiving slit. The XRD patterns of bulk rocks were collected from 3° to 65° 2θ, and the XRD patterns for clay fractions were recorded from 3° to 30° 2θ. The NEWMOD program was used to fit the XRD patterns of clay fractions in the EG treatment, in order to identify mixed-layer clay minerals and determine the proportion and structure of each clay mineral present.

2.3. Electron energy loss spectroscopy (EELS)

EELS was performed at Wuhan University using a JEOL JEM-ARM200F microscope operated at 200 kV with a Schottky cold-field emission gun. The spectra of the Ti L-edge were acquired at an energy of 453-488 eV and exposure time of 1.0 s, and their backgrounds were subtracted. The energy resolution of EELS spectroscopy is 0.4 eV. The calculation of the average valence state of Ti was based on the intensity of the L_2 and L_3 peaks in the EELS spectrum, according to the following equation from Zanetta et al. (2023):

$$Y = -1.985\,X^2 - 3.531\,X + 6.297 \quad (1)$$

In this equation, Y represents intensity of the L_3 peak *t*, while X denotes the amount of tetravalent titanium (Ti^{4+}) as a proportion of total titanium.

2.4. Micromorphology analysis (SEM and TEM)

Representative altered volcanic ash samples were selected for preparation of polished thin sections, which were then carbon-coated for enhanced electrical conductivity for use in scanning electron microscopy (SEM). SEM observations were made on a HITACHI-SU8010 field-emission scanning electron microscope at the China University of Geosciences (Wuhan) at an accelerating voltage of 15 kV, in the back-scattered emission mode with EDS to identify Ti minerals.

Transmission electron microscopy (TEM) of the morphology of authigenic anatase was undertaken in combination with focused ion beam (FIB) technology, which allows better preservation of textural features and spatial relationships among nano-scale minerals (Fig. 3). The procedure for extracting FIB sections was as

follows: (1) An ultra-thin section of the sample was created using the FIB system (Helios G4 CX, ThermoFisher Scientific) at the State Key Laboratory of Geological Processes and Mineral Resources (GPMR) in the China University of Geosciences (Wuhan); (2) A predefined area (~20 μm^2) was coated with platinum (Pt), and the surroundings cut down to a depth of ~10 μm using a gallium (Ga) ion beam. (3) Afterwards, the resulting foil was picked up by an EasyLift in-situ tungsten (W) probe inside the FIB and then mounted on a TEM copper (Cu) grid (Omniprobe, Oxford Instrument). (4) The extracted samples were thinned to ~100 nm using a Ga ion beam at 30 kV with beam currents ranging from 9.3 nA to 80 pA and at 5 kV with a beam current of 43 pA and 2 kV with a beam current of 23 pA for the final processing. Transmission electron microscopy observation and EDX analysis was performed on a Talos F200X G2 TEM field-emission transmission electron microscope operated at an accelerating voltage of 200 kV with a line resolution less than 0.10 nm.

2.5. Major- and trace-element analyses

Major-element compositions of bulk-rock samples were obtained using X-ray fluorescence (XRF) spectroscopy. Fused pellets were prepared by addition of 5 g of dilithium tetraborate to 1 g of the dried sample powder (<74 μm). This mixture was homogenized and was further mixed with four drops of 1.5% LiBr. Subsequently, the fused pellets were produced using a hydraulic press and heated by a Philips Perl'X automatic bead machine. XRF analysis was then undertaken using a Shimadzu XRF-1800 sequential spectrometer at Wuhan SampleSolution Analytical Technology Co., Ltd. Loss-on-ignition (LOI) was calculated as the difference in sample weight after heating to 1000 °C. The relative standard deviation of major elements was usually < 1%, and the detection limit was generally about 0.01%.

Trace-element and rare-earth element (REE) concentrations were measured using an Agilent 7700e inductively coupled plasma mass spectrometer (ICP-MS) at SampleSolution Analytical Technology Company (Wuhan). The sample preparation procedure consisted of the following steps: (1) adding about 50 mg of dried altered volcanic ash powder sample to a Teflon bomb and wetting it with a few drops of ultra-pure water. (2) Mixing a solution of 1.5 mL HNO_3 and 1.5 mL HF, sealing the bomb, and heating it to 190 °C in an electric oven for 48 h. (3) Evaporating the sample

completely at 115 °C and then adding 1 mL HNO_3 solution to the residue. (4) Dissolving the residual material in 3 mL 30% HNO_3 solution, sealing the Teflon bomb, and heating it to 190 °C for 16 h. (5) Diluting the solution to 100 mL with 2% HNO_3 solution. The relative standard deviations for REEs and Y were usually less than 4% and for other trace elements usually less than 10%.

The weathering degree of the samples was determined using chemical weathering indices: the chemical index of weathering (CIW; Harnois, 1988) and the Ruxton ratio (R; Ruxton, 1968), based on the bulk chemical results of the samples:

$$CIW = Al_2O_3 / (Na_2O + Al_2O_3 + CaO^*) \quad (2)$$

$$R = SiO_2/Al_2O_3 \quad (3)$$

In these equations, all the element oxides are given in molar units, and CaO* represents calcium in the silicate fraction only.

2.6. Major-element data compilation and meta-analysis of global (K-)bentonites

We assembled a geochemical dataset comprising 384 (K-)bentonite samples (in particular those from sedimentary successions) from 40 sections to assess the potential influence of chemical weathering on the illitization of smectite and the joint influence of chemical weathering and illitization on the formation of Ti-oxides. We assumed that Ti is present mainly in Ti-oxides and, thus, that TiO_2 concentration data reflect Ti-oxide content in (K-)bentonites. We also assumed that all (K-)bentonites have undergone significant weathering and diagenesis, and, thus, that feldspars represent a minor mineral phase, and that clay minerals and illite are the main contributors to Al_2O_3 and K_2O, respectively. Source literature is listed in Table 1.

Pearson's *r* and a *p* value threshold of 0.05 were used to evaluate the statistical significance of chemical weathering effects on (K-)bentonite variables, or of K_2O content on Ti-oxide formation. Samples were grouped based on depositional environment and dominant clay species, with relationships among samples displayed as a forest plot. Line regression analysis was also used to visualize the correlation among chemical weathering indexes and the contents of K_2O and TiO_2.

3. Results

3.1. XRD analysis of clay minerals and peak fitting

X-ray diffraction (XRD) patterns reveal that altered volcanic ash samples predominantly consist of interstratified illite-smectite (I-S), with minor amounts of quartz, albite, gypsum, jarosite, pyrite, anatase, and occasionally kaolinite, illite and bassanite (Fig. 4a). Gypsum and jarosite are abundant in samples L260 and L266 but were not detected in sample L271. Anatase is identified by its (101) reflection at a peak of 3.51 Å in XRD diffractograms. Our results indicate that I-S is the dominant phase in the clay fraction of volcanic ash samples (Fig. 4b): the strong peak at ~11.3 Å in the air-dried clay fraction (AD) XRD patterns is split into two peaks at ~12.2 Å and ~9.4 Å after EG saturation. Additionally, trace amounts of illite and kaolinite can be seen in samples L264, L266, and L271 (Fig. 4b).

We conducted peak fitting of XRD patterns for determination of clay-mineral composition and calculation of illite-layer percentage (I%) in I-S (Fig. 5). This fitting process focuses only on the reflections generated by clay minerals, and it disregards non-clay peaks unless these peaks overlap with clay mineral peaks. We selected illite-smectite, illite and kaolinite for peak fitting, and we applied the same particle-orientation parameter ($\sigma^* = 6.68$) to all phases. The stacking sequence of I-S was characterized as "Reichweite (R)", which is commonly in the range of 0 to 3 (Jagodzinski, 1949; Wang and Wang, 2021). To optimize results, the crystallinity of each phase, I% in I-S, and other parameters such as octahedral-site iron content in the illite layer and water content of the smectite layer were adjusted manually until we achieved the best fit of theoretical patterns to the experimental data. The final NEWMOD results are shown in Figure 4, and the main fitting parameters are listed in Table 2.

The best-fit results of the altered volcanic ash samples demonstrate that the stacking sequence of I-S is regular (ISIS), and that two types of I-S clay with different I% (i.e., one with a lower I% of 64%, and the other with a higher I% of 76%) are present in samples L255 to L271. The experimental pattern of L277 can be modeled with a single type of I-S with 76% illite layers. Within samples L264, L266, and L271, the amount of kaolinite and illite present is minor (less than 4%). The

percentage of I-S clay with a high I% shows a general increase upward from the bottom layer (L255, 53%) to the top layer (L277, 100%), which is also mirrored in increases in the coherent scattering domain size (CSDS) of I-S (from 5.14 to 9.41).

3.2. The occurrence of Ti-oxide minerals and their spatial relationship to I-S

The altered volcanic ash samples contain both discrete microscale Ti-bearing phases and nanoscale anatase crystals (Figs. 6-8). The microscale Ti-bearing phases, which have irregular outlines with a grain size ranging from 12 to 64 μm (Fig. 6), are frequently composed of clusters of smaller TiO_2 particles (Fig. 6b). SEM-EDS mapping shows that detrital Ti-bearing grains with straight edges exhibit Zr enrichment in their fine cracks and rims, whereas the central area of the grains is mainly composed of Ti with only trace amounts of Zr (Fig. 6a-c). Such characteristics suggest that the larger Ti-bearing phases are possibly srilankite. The irregularly shaped srilankite grains have a relatively homogeneous distribution of Ti and Zr in their centers, but their rims consist of Zr-enriched zones with intense leaching of Ti (Fig. 6d-f).

The nanoscale titanium minerals (100-400 nm in size) are primarily composed of Ti-oxides, as indicated by EDS analysis (Fig. 7). The SAED pattern shows characteristic diffraction spots of anatase (<112> and <301>) (Fig. 7d). These anatase particles exhibit euhedral tetragonal dipyramid morphologies, and some have relatively round crystal edges and faces, likely due to a low degree of Ti supersaturation (Cornu et al., 1999; Hong et al., 2019a). The EELS spectrum of Ti in Ti-oxide particles (Fig. 7e) exhibits two prominent lines (L_2 and L_3 edges), resulting from core-hole spin-orbit coupling. These two lines subsequently undergo a further splitting into four lines, attributed to the influence of the octahedral crystal field on the *3d* states (Radtke et al., 2006). The distinctive shape and L_2-to-L_3 ratio in the EELS spectrum are characteristic features of titanium dioxide (TiO_2) (Fig. 7e, f), which has an average valence of +3.5. This suggests that most of the Ti exists in a quadrivalent state (+4), with a small fraction of Ti in a lower valence state.

SEM images of the altered volcanic ash samples reveal that I-S has a platy habit and curved edges (Fig. 8a-b), with a thickness range of 15-25 nm. I-S is dominant under SEM, consistent with the XRD results. High-resolution TEM images of anatase particles show that I-S grows parallel to the crystal surface of anatase, with a fringe spacing of either 10 Å or 11 Å (Fig. 8c-e). The 10 Å spacing is attributed to the lattice fringe of illite layers, whereas the 11 Å spacing corresponds to partially collapsed smectite layers following electron irradiation. Newly formed TiO_2 crystals with spherical outlines were also found closely associated with the I-S clays (Fig. 8f).

3.3. Geochemical compositions of the altered volcanic ash samples

The major-element compositions and weathering indices (SiO_2/Al_2O_3 and CIW) of the Xiakou altered volcanic ash samples are listed in Table 3. The CIW values range from 94 to 99, with a mean of 97. The SiO_2/Al_2O_3 values range from 3.55 to 4.25 (mean 3.80) and do not covary significantly with other weathering indices. The lowest value is found in sample L271, whereas the highest is found in sample L264 (n.b., higher SiO_2/Al_2O_3 denotes lower weathering intensity).

The total concentrations of rare earth elements (ΣREE) of the Xiakou altered volcanic ash range from 69.7 to 284 ppm (Table 4). Their REE distributions show an enrichment in light rare earth elements (LREEs) and a slight depletion of heavy rare earth elements (HREEs), resulting in a right-leaning profile for LREEs and a relatively flat pattern for HREEs, similar to that of felsic (K-)bentonites from the Meishan, Chaotian, Shangsi, Rencunping, and Dongpan sections (He et al., 2014) (Fig. 9). A weak but distinct negative Eu anomaly can also be observed. In comparison to other (K-)bentonite samples, L264 has a notably lower ΣREE of 70 ppm (versus 192-284 ppm for other samples) and a lower ΣLREE/ΣHREE of 2.94 (versus 3.73-9.28 for other samples).

3.4. Meta-analysis of (K-)bentonite major-element data

To provide an evaluation on the influence of chemical weathering on the illitization process, we used two weathering indices, namely CIW (i.e., CIA without K_2O) and SiO_2/Al_2O_3 for cross-validation (Fig. 10). The forest plot for bentonite samples deposited in various settings shows a significant increase in K_2O with

weathering intensity, as reflected in significant correlations of K_2O with CIW and SiO_2/Al_2O_3. This statistical relationship also extends to bentonite samples deposited in many other types of environments (deep marine and lacustrine environment), but it is particularly evident in shallow-marine facies. In bentonite samples deposited in paludal settings, K_2O content is positively correlated with SiO_2/Al_2O_3 (r = +0.90, 95% CI: +0.79 to +0.96, p <0.01), which is different from the results of bentonite from other environments (shallow marine, deep marine, and lacustrine environments). This divergent relationship of K_2O content to weathering intensity among depositional settings or dominant clay species may be due to the different transformation pathways of clay minerals. Volcanic ash deposited in an acidic paludal environment (paludal) is unstable and will alter into kaolinite rather than I-S clay. Thus, potassium in the clay mineral structure is not "fixed", but rather can be leached out as weathering continues.

The influence of chemical weathering on K_2O content is also regulated by the dominant clay species in a (K-)bentonite. Specifically, the positive relationship of chemical weathering with K_2O content is observed only for (K-)bentonites that dominantly consist of I+S or I-S, and that have undergone some degree of illitization. Meta-analysis shows that K_2O content is positively correlated with TiO_2 content in samples from shallow-marine and paludal settings, suggesting that illitization of smectite can increase the Ti content of (K-)bentonites deposited in these environments. Additionally, (K-)bentonite samples dominated by I-S phases exhibit a more significant positive correlation between K_2O and TiO_2 than bentonite dominated by other clay species.

To better decipher genetic relationships among chemical weathering, smectite illitization, and Ti-oxide formation, we generated various geochemical crossplots for shallow-marine (K-)bentonites. The K_2O-TiO_2 crossplot (Fig. 11a) shows that the concentrations of TiO_2 and K_2O are 0-2.5 wt.% and 0-10 wt.%, respectively, with a degree of positive covariation between them. The K_2O-CIW and K_2O-SiO_2/Al_2O_3 crossplots (Fig. 11b, 11c) show opposite trends, which confirm the reliability of the two weathering indices (i.e., CIW and Ruxton value). The Al_2O_3-TiO_2 crossplot (Fig. 11d) shows a significant positive correlation of TiO_2 content with Al_2O_3 (r = +0.41, p

<0.01), probably due to association of both oxides with clay minerals.

4. Discussion

4.1. Weathering of Ti-bearing minerals and formation of anatase in (K-)bentonite

Titanium, apart from being found in titanium dioxide, can also be found in various minerals, including primary silicate minerals such as biotite, muscovite, and hornblende, as well as pseudobrookite, srilankite, and perovskite (Baioumy, 2014; Schulz et al., 2016). In sedimentary rocks, the Ti-oxide minerals anatase and brookite are common Ti-bearing phases, while rutile tends to dominate in metamorphic rocks formed at higher pressures and temperatures (Table 5) (Morad and Aldahan, 1982; Morad, 1988; Schroeder and Shiflet, 2000; Allo, 2004; Papoulis et al., 2009; Baioumy, 2014; Liu et al., 2019).

According to our SEM and TEM results, the Ti-oxides in the altered volcanic ashes at Xiakou occur as relatively large srilankite crystals and fine-grained anatase crystals. The srilankite crystals display straight outlines with broken edges, suggesting a detrital origin. Generally, detrital titanium minerals originating from terrestrial sources are rare in marine sediments due to their high density (3.8-4.3 g/cm^3), and they usually have a rounded shape as a result of physical erosion during transport (Baioumy, 2014). However, the srilankite grains in the bentonite samples display a low roundness, indicating that they have experienced only limited transport and may have originated from a magmatic source rather than a sedimentary one. The lack of Zr in the little grains around the altered srilankite and the enrichment of Zr on the margins of the srilankite crystals lead us to infer that, during the alteration process, Ti was partly leached from the margins of the srilankite and subsequently reprecipitated as TiO_2 crystals.

The nanoscale anatase crystals observed by HRTEM have a relatively euhedral tetragonal dipyramidal shape with no signs of erosion, suggesting an authigenic origin (Fig. 7). Both discrete crystals and aggregates are present within the altered volcanic ashes. Generally, anatase is rare in marine sediments because of the low concentration of dissolved titanium in these environments (Skrabal, 2006; Liu et al., 2019). For this reason, the formation of anatase in altered volcanic ash is attributable to the

breakdown of detrital Ti-bearing precursors such as biotite (Papoulis et al., 2009), ilmenite (Allo, 2004; Schulz et al., 2016), and titanite (Novoselov et al., 2020).

The petrological, mineralogical and geochemical analyses suggest that three main Ti-bearing precursors were responsible for the formation of anatase: srilankite, plagioclase, and clay minerals. As indicated by SEM, the alteration of srilankite released Ti, which was the main source of Ti for the formation of anatase (Fig. 6). Plagioclase, which was identified in bulk-rock diffractograms (Fig. 4), contains trace amounts of Ti in its structure that can be released during alteration (Papoulis et al., 2009). In addition, Ti in octahedral sites or interlayer spaces of smectite formed via weathering of volcanic glass can also be released during the illitization process (Fig. 12).

4.2. The influence of chemical weathering on the illitization of smectite in (K-)bentonite

During the post-depositional and early diagenetic stages, volcanic ash devitrification results in release of alkalis and Si, while also leading to uptake of Mg, Fe, and Ca (Christidis, 1995). At the same time, unstable volcanic glass will be readily weathered to smectitic minerals, which will subsequently transform into I-S (Cuadros and Altaner, 1998; Fisher and Schmincke, 2012). Due to incorporation of potassium ions into smectite, the illitization process is similar to reverse weathering (Isson and Planavsky, 2018; Aubineau et al., 2019).

The consistent R1 stacking structure and the narrow range of I% in the I-S minerals of these bentonite samples (from layer L255 to L277 with I % range from 62 % to 77 %), together with the stratigraphic proximity of all of the bentonite samples, suggest that they share a similar diagenetic history. Based on a correlation between I-S expandable layer content and burial temperature (Sucha et al., 1993), the maximum burial temperature of the Permian-Triassic succession at Xiakou was lower than 180 °C. This result is much higher than temperatures (50-90 °C) inferred from low conodont alteration index (CAI) values at Xiakou (Du et al., 1983; Shen et al., 2013). Such a mismatch was also reported by Derkowski et al. (2021), who showed that the maximum paleotemperatures obtained from illite-smectite analysis greatly exceeded those predicted by lipid biomarkers. They attributed this discrepancy to the

influence of K-bearing hot fluids on the illitization process. However, the Xiakou area, being a carbonate platform, does not show any indications of hot fluid intrusion based on its mineralogical and chemical compositions. Rather, we think that this temperature discrepancy may be attributable to factors (such as chemical weathering) that could potentially enhance the illitization reaction.

K^+ within illite or I-S clay is fixed in the interlayer site of illite layers. Total K content in I-S clays can reach 7.0 wt.% (Weaver and Pollard, 1973), indicating the presence of a large amount of illitic clays or illitic layers (Hong et al., 2019b). The forest plot that illustrates the effect of chemical weathering on the content of K_2O (Fig. 10) implies that the correlation between K_2O and degree of chemical weathering is exclusively positive for samples dominated by I-S clays. These findings suggest that the chemical weathering process can modulate K_2O content in bentonite samples by modifying the proportion of illite layers.

The illitization process in (K-)bentonites results in an increasing proportion of illite layers, thus increasing K_2O content (Huff and Tuerkmenoglu, 1981; Bozkaya et al., 2016). Chemical weathering of (K-)bentonites can change their degree of illitization and, hence, levels of K_2O enrichment. The extent of illitization is governed by both diagenetic temperatures and the duration of this process (Somelar et al., 2009). The alteration process itself is influenced by various factors including the composition of the volcanic ash, the water-to-rock ratio, and the chemical composition of diagenetic fluids (Christidis, 1998). Considering the close proximity of bentonite layers within a single stratigraphic profile, it is reasonable to assume that they share similar diagenetic conditions and comparable burial times. Consequently, the critical determinants of the illitization process lie with fluid chemistry and water:rock ratio. As chemical weathering proceeds, elements such as Mg, K, and Ca are released from the parent material due to their greater chemical reactivity (Loughnan, 1969). The resulting changes in fluid chemistry, particularly the increased availability of porewater K^+, along with elevated water:rock ratios, have the potential to enhance the illitization process.

The relationship between K_2O content and the CIW or Ruxton value in (K-)bentonite varies under different environmental conditions (Fig. 10a-b). This

observation implies that the influence of chemical weathering on illitization is also governed by the nature of the depositional environment. A robust correlation between weathering intensity and K_2O content is evident in bentonite deposits within shallow-water facies. Conversely, bentonite deposited in lacustrine, paludal, and deep-marine environments exhibit a weaker correlation. This characteristic can be attributed to the diverse weathering conditions observed among different sedimentary environments. For instance, the shallow-marine setting exhibits relatively turbulent hydrodynamic conditions, facilitating the mixing of volcanic ash with terrestrial inputs. Nearby continental weathering can generate the K^+ required for illitization and transport it to the ocean via river systems, ultimately influencing the chemical composition of bentonite porewaters, thus modulating the extent of the illitization process.

4.3. The illitization process controls Ti mineralization in (K-)bentonites

Under supergene conditions, titanium can be released from parent materials in the form of $Ti(OH)_4$ colloids in acidic (pH<3), organic-rich environments such as paludal and lacustrine settings and precipitate as TiO_2 when pH is higher than 5 (Craig and Loughnan, 1964; Brookins, 2012; Hong et al., 2020). The enriched LREEs and high LREE/HREE ratios (mean 5.75) in most of the altered volcanic ashes at Xiakou suggest alteration in an acidic environment (Lee and Byrne, 1992). An acidic environment is also evidenced by the occurrence of jarosite in most of the volcanic ash layers, because the formation of this mineral is thought to require an acidic environment (Baccolo et al., 2021). The presence of jarosite only in the bentonite layers excludes the possibility of a detrital origin for this mineral.

An acidic environment allows for mobilization of Ti and its subsequent transport through bentonite porewaters. Moreover, the illitization process can create zones of overpressure that drive out hydrocarbons and water, leading to higher porosity in the rock matrix (Pytte and Reynolds, 1989). Chemical weathering leads to enhanced permeability of the parent rock, linked to dissolution of more weatherable components such as feldspar and biotite (Tuğrul, 2004). The relatively high degree of illitization in the Xiakou altered volcanic ashes, as revealed by the high content of illite layers in I-S, provides evidence of a more permeable condition, facilitating transport of Ti through pore spaces.

Formation of authigenic anatase in Xiakou altered volcanic ash was found to be closely associated with I-S clays: most of the anatase crystals grow on the surface of I-S clays rather than in pore spaces. Due to their small particle size (<2 μm) and complex pore structure, these clays have the potential to adsorb various metal cations (Uddin, 2017), and their high specific surface areas provide suitable nucleation sites for formation of anatase. The close relationship between Ti and I-S suggests that a large proportion of the Ti released from Ti-bearing precursors was likely adsorbed by I-S clays and then reprecipitated as anatase on their surfaces when the local chemical micro-environment became more alkaline (Fig. 12). This hypothesis is also supported by the growth relationship between I-S clays and anatase observed in TEM images (Fig. 8).

Our data compilation for (K-)bentonites suggests that, except for those formed in lacustrine environments, a significant positive correlation between K_2O and TiO_2 is typical (Fig. 10). Significantly, this positive correlation is found only in (K-)bentonites dominated by I-S clays rather than by other clay-mineral species. The statistical evidence presented herein substantiates the idea that the illitization process, or the formation of I-S clay, potentially plays a role in the enrichment of titanium (Ti), possibly through growth of TiO_2 minerals on the clay structure (Zhou et al., 2012).

5. Implications

The illitization of smectite is a common process in sedimentary and hydrothermal systems. In sedimentary systems, illitization is regarded as being mediated by temperature- and depth-dependent diagenetic processes. The degree of illitization is often used to reconstruct the thermal history of sedimentary basins and to prospect for oil and gas. Our study provides evidence that chemical weathering can occur throughout the entire alteration process of volcanic ashes in the surface to near-surface environment, influencing illitization reactions by changing fluid composition and ash-layer porosity and permeability characteristics. Strong associations between authigenic anatase and I-S clays (at the micro scale and macro scale) provide evidence of a previously under-appreciated precipitation pathway, enhancing our understanding of the formation mechanisms of authigenic anatase in (K-)bentonites, and establishing

a link between the alteration of clay minerals and the creation of nano-minerals. Our finding could serve as a valuable reference point for future investigations into the mechanisms of nano-mineral formation, and the proposed mechanism could be strengthened by additional thermodynamic analysis or chemical experiment.

Anatase, an exceptional semiconducting mineral with outstanding photocatalytic capabilities, particularly at the nanoscale, is also a crucial raw material for semiconductors. Our study demonstrates that in sedimentary systems, this mineral can form through the weathering and diagenetic transformation of clay minerals, providing a fresh perspective on the resource aggregation effect of mineral weathering. Moreover, while TiO_2 in sediments is generally regarded as immobile and has often been used for parent-rock discrimination, our research findings suggest that titanium can migrate out of the crystal lattice of the parent mineral in a semi-open system characterized by well-developed porosity and where water-rock interactions and mineral weathering processes occur easily. Some of the titanium remains within the porewater system, forming nano-scale anatase, while another portion of the titanium may be leached from the system. Therefore, it is important to exercise caution when using titanium for evaluation of the genesis of a volcanic ash.

Acknowledgments

This work was supported by the National Natural Science Foundation of China (Projects 41972040, 42172045, 42002042 and 42102031), the Fundamental Research Funds for the Central Universities, China University of Geosciences (Wuhan) (No. CUG170106).

References

Allo, W., 2004. Authigenic Ti-bearing crystals in a Precambrian clay from Buenos Aires Province, Argentina. Clays and Clay Minerals, 52(3), 304-310.

Astini, R.A., Collo, G., Martina, F., 2007. Ordovician K-bentonites in the upper-plate active margin of Western Gondwana, (Famatina Ranges): Stratigraphic and palaeogeographic significance. Gondwana Research, 113, 311-325.

Aubineau, J., El Albani, A., Bekker, A., Somogyi, A., Bankole, O.M., Macchiarelli, R., Meunier, A., Riboulleau, A., Reynaud, J., Konhauser, K.O., 2019.

Microbially induced potassium enrichment in Paleoproterozoic shales and implications for reverse weathering on early Earth. Nature Communications, 10(1), 2670.

Baccolo, G., Delmonte, B., Niles, P.B., Cibin, G., Di Stefano, E., Hampai, D., Keller, L., Maggi, V., Marcelli, A., Michalski, J., Snead, C., Frezzotti, M., 2021. Jarosite formation in deep Antarctic ice provides a window into acidic, water-limited weathering on Mars. Nature Communications, 12(1).

Baioumy, H.M., 2014. Ti-bearing minerals in sedimentary kaolin deposits of Egypt. Applied Clay Science, 101, 345-353.

Batchelor, R.A., 2014. Geochemistry of Upper Ordovician metabentonites and their cognate apatite microphenocrysts from Norway and Sweden. GFF, 136(2), 387-397.

Batchelor, R.A., Jeppsson, L., 1999. Wenlock metabentonites from Gotland, Sweden; geochemistry, sources and potential as chemostratigraphic markers. Geological Magazine, 136(6), 661-669.

Bozkaya, Ö., Günal-Türkmenoğlu, A., Göncüoğlu, M.C., Ünlüce, Ö., Yilmaz, İ.Ö., Schroeder, P.A., 2016. Illitization of Late Devonian-Early Carboniferous K-bentonite from Western Pontides, NW Turkey: Implications for their origin and age. Applied Clay Science, 134, 257-274.

Brookins, D.G., 2012. Eh-pH Diagrams for Geochemistry. Springer Science & Business Media.

Cai, L., Tong, M., Wang, X., Kim, H., 2014. Influence of clay particles on the transport and retention of titanium dioxide nanoparticles in quartz sand. Environmental Science & Technology, 48(13), 7323-7332.

Chaikovskiy, I.I., Chaikovskaya, E.V., Korotchenkova, O.V., Chirkova, E.P., Utkina, T.A., 2019. Authigenic titanium and zirconium minerals at the Verkhnekamskoe salt deposit. Geochemistry International, 57(2), 184-196.

Cheng, C., Xiao-Ying, S., Yun-Feng, F., Xin-Jiang, W., 2012. K-bentonites from the Jinsushan Formation of Late Ordovician, southern Ordos Basin: SHRIMP dating and tectonic environment. Geoscience, 26(2), 205-219.

Christidis, G.E., 1995. Mechanism of illitization of bentonites in the geothermal field

of Milos Island Greece: Evidence based on mineralogy, chemistry, particle thickness and morphology. Clays and Clay Minerals, 43(5), 569-585.

Christidis, G.E., 1998. Comparative study of the mobility of major and trace elements during alteration of an andesite and a rhyolite to bentonite, in the islands of Milos and Kimolos, Aegean, Greece. Clays and Clay Minerals, 46(4), 379-399.

Condie, K.C., 1978. Geochemistry of Proterozoic granitic plutons from New Mexico, USA. Chemical Geology, 21(1-2), 131-149.

Cornu, S., Lucas, Y., Lebon, E., Ambrosi, J.P., Luizão, F., Rouiller, J., Bonnay, M., Neal, C., 1999. Evidence of titanium mobility in soil profiles, Manaus, central Amazonia. Geoderma, 91(3), 281-295.

Craig, D.C., Loughnan, F.C., 1964. Chemical and mineralogical transformations accompanying the weathering of basic volcanic rocks from New South Wales. Soil Research, 2(2), 218-234.

Cuadros, J., Altaner, S.P., 1998. Characterization of mixed-layer illite-smectite from bentonites using microscopic, chemical, and X-ray methods: Constraints on the smectite-to-illite transformation mechanism. American Mineralogist, 83(7-8), 762-774.

Dainyak, L.G., Drits, V.A., Zviagina, B.B., Lindgreen, H., 2006. Cation redistribution in the octahedral sheet during diagenesis of illite-smectites from Jurassic and Cambrian oil source rock shales. American Mineralogist, 91(4), 589-603.

Derkowski, A., Środoń, J., Goryl, M., Marynowski, L., Szczerba, M., Mazur, S., 2021. Long-distance fluid migration defines the diagenetic history of unique Ediacaran sediments in the East European Craton. Basin Research, 33(1), 570-593.

Dill, H.G., 2010. Authigenic heavy minerals a clue to unravel supergene and hypogene alteration of marine and continental sediments of Triassic to Cretaceous age (SE Germany). Sedimentary Geology, 228(1-2), 61-76.

Du, G.Q., 1983. On the color alteration of conodonts and maturity of organic matter in the Permian and Triassic systems, Hubei. Acta Petrolei Sinica, 4, 11–18 (in Chinese with English abstract).

Ece, O.I., Nakagawa, ZE., Schroeder, P.A. Alteration of volcanic rocks and genesis of

kaolin deposits in the Şile region, northern Istanbul, Turkey. I: Clay mineralogy. Clays and Clay Minerals, 51, 675–688 (2003).

Fisher, R.V., Schmincke, H., 2012. Pyroclastic Rocks. Springer Science & Business Media.

Gong, N., Hong, H., Huff, W.D., Fang, Q., Bae, C.J., Wang, C., Yin, K., Chen, S., 2018. Influences of sedimentary environments and volcanic sources on diagenetic alteration of volcanic tuffs in South China. Scientific Reports, 8(1), 7616.

Harnois, L., 1988. The CIW index: A new chemical index of weathering. Sedimentary Geology, 55(3), 319-322.

He, B., Zhong, Y., Xu, Y., Li, X., 2014. Triggers of Permo-Triassic boundary mass extinction in South China: The Siberian Traps or Paleo-Tethys ignimbrite flare-up? Lithos, 204, 258-267.

Hong, H., Fang, Q., Wang, C., Churchman, G.J., Zhao, L., Gong, N., Yin, K., 2017. Clay mineralogy of altered tephra beds and facies correlation between the Permian-Triassic boundary stratigraphic sets, Guizhou, south China. Applied Clay Science, 143, 10-21.

Hong, H.L., Algeo, T.J., Fang, Q., Zhao, L., Ji, K., Yin, K., Wang, C., Cheng, S., 2019a. Facies dependence of the mineralogy and geochemistry of altered volcanic ash beds: An example from Permian-Triassic transition strata in southwestern China. Earth-Science Reviews, 190, 58-88.

Hong, H.L., Zhao, L., Fang, Q., Algeo, T.J., Wang, C., Yu, J., Gong, N., Yin, K., Ji, K., 2019b. Volcanic sources and diagenetic alteration of Permian-Triassic boundary K-bentonites in Guizhou Province, South China. Palaeogeography, Palaeoclimatology, Palaeoecology, 519, 141-153.

Hong, H., Jing, X., Wang, M., Ji, K., Liu, C., Algeo, T.J., Fang, Q., 2020. Occurrence of anatase in reworking altered ash beds (K-bentonites and tonsteins) and discrimination of source magmas; a case study of terrestrial Permian-Triassic boundary successions in China. Clay minerals, 55(4), 329-341.

Huang, H., Cawood, P.A., Hou, M., Ni, S., Yang, J., Du, Y., Wen, H., 2018. Provenance of Late Permian volcanic ash beds in South China: Implications for

the age of Emeishan volcanism and its linkage to climate cooling. Lithos, 314-315, 293-306.

Huff, W.D., 2016. K-bentonite; a review. The American Mineralogist, 101(1), 43-70.

Huff, W.D., Tuerkmenoglu, A.G., 1981. Chemical characteristics and origin of Ordovician K-bentonite along the Cincinnati Arch. Clays and Clay Minerals, 29(2), 113-123.

Huff, W.D., Kolata, D.R., Bergstrom, S.M., Zhang, Y.S., 1996. Large-magnitude Middle Ordovician volcanic ash falls in North America and Europe; dimensions, emplacement and post-emplacement characteristics. Journal of Volcanology and Geothermal Research, 73(3-4), 285-301.

Huff, W.D., Bergstrom, S.M., Kolata, D.R., Cingolani, C.A., Astini, R.A., 1998. Ordovician K-bentonites in the Argentine Precordillera; relations to Gondwana margin evolution, *in* Pankhurst, R.J., Raela, C.W. (eds.), The Proto-Andean Margin of Gondwana, Geological Society of London Spec. Publ. 142, 107-126.

Isson, T.T., Planavsky, N.J., 2018. Reverse weathering as a long-term stabilizer of marine pH and planetary climate. Nature, 560(7719), 471-475.

Jackson, M.L.,1978. Soil Chemical Analyses. Authors' publication, Univ. of Wisconsin Madison, USA.

Jagodzinski, H., 1949. Eindimensionale Fehlordnung in Kristallen und ihr Einfluss auf die Röntgeninterferenzen. I. Berechnung des Fehlordnungsgrades aus den Röntgenintensitäten. Acta Crystallographica, 2(4), 201-207.

Kadir, S., Külah, T., Erkoyun, H., Uyanık, N.Ö., Eren, M., Elliott, W.C., 2021. Mineralogy, geochemistry, and genesis of bentonites in Upper Cretaceous pyroclastics of the Bereketli member of the Reşadiye Formation, Reşadiye (Tokat), Turkey. Applied Clay Science, 204, 106024.

Kiipli, Tarmo, Kallaste, Toivo, Nielsen, Arne, T., Schovsbo, Niels, H., 2014. Geochemical discrimination of the Upper Ordovician Kinnekulle Bentonite in the Billegrav-2 drill core section, Bornholm, Denmark. Estonian Journal of Earth Sciences, 63(4), 264-270.

Lee, J.H., Byrne, R.H., 1992. Examination of comparative rare earth element complexation behavior using linear free-energy relationships. Geochimica et

Cosmochimica Acta, 56(3), 1127-1137.

Liao, Z., Hu, W., Cao, J., Wang, X., Yao, S., Wu, H., Wan, Y., 2016. Heterogeneous volcanism across the Permian-Triassic Boundary in South China and implications for the Latest Permian Mass Extinction: New evidence from volcanic ash layers in the Lower Yangtze Region. Journal of Asian Earth Sciences, 127, 197-210.

Liu, Z.R., Zhou, M., Williams-Jones, A.E., Wang, W., Gao, J., 2019. Diagenetic mobilization of Ti and formation of brookite/anatase in early Cambrian black shales, South China. Chemical Geology, 506, 79-96.

Loughnan, F.C., 1969. Chemical Weathering of the Silicate Minerals. Elsevier, New York, 154 pp.

Lowe, D.J., 2011. Tephrochronology and its application: A review. Quaternary Geochronology, 6(2), 107-153.

Lu, Q., Lei, X.R., Liu, H.F., 1991. Genetic types and crystal chemical classification of irregular illite/smectite interstratified clay minerals. Acta Mineralogica Sinica, 11(2), 97-104.

Malitch, K.N., Belousova, E.A., Griffin, W.L., Badanina, I.Y., Pearson, N.J., Presnyakov, S.L., Tuganova, E.V., 2010. Magmatic evolution of the ultramafic-mafic Kharaelakh intrusion (Siberian Craton, Russia): insights from trace-element, U-Pb and Hf-isotope data on zircon. Contributions to Mineralogy and Petrology, 159(6), 753-768.

Moore, D.M., Reynolds, R.C., Jr., 1989. X-ray Diffraction and the Identification and Analysis of Clay Minerals. Oxford University Press, Oxford, UK.

Morad, S., 1988. Diagenesis of titaniferous minerals in Jurassic sandstones from the Norwegian Sea. Sedimentary Geology, 57(1-2), 17-40.

Morad, S., Aldahan, A.A., 1982. Authigenesis of titanium minerals in two Proterozoic sedimentary rocks from southern and central Sweden. Journal of Sedimentary Petrology, 52(4), 1295-1305.

Novoselov, A.A., Silva, D., de Souza Filho, C.R., 2020. Authigenic titanite in weathered basalts: Implications for paleoatmospheric reconstructions. Geoscience Frontiers, 11(6), 2183-2196.

Papoulis, D., Tsolis-Katagas, P., Kalampounias, A.G., Tsikouras, B., 2009. Progressive formation of halloysite from the hydrothermal alteration of biotite and the formation mechanisms of anatase in altered volcanic rocks from Limnos Island, northeast Aegean Sea, Greece. Clays and Clay Minerals, 57(5), 566-577.

Pytte, A.M., Reynolds, R.C., 1989. The thermal transformation of smectite to illite, *in* Naeser, N.D., McCulloh, T.H. (eds.), Thermal History of Sedimentary Basins. Springer, New York, pp. 133-140.

Radtke, G., Lazar, S., Botton, G.A., 2006. High-resolution EELS investigation of the electronic structure of ilmenites. Physical Review B, Condensed Matter and Materials Physics, 74(15), 155117.

Ruggieri, F., Fernandez-Turiel, J.L., Saavedra, J., Gimeno, D., Polanco, E., Amigo, A., Galindo, G., Caselli, A., 2012. Contribution of volcanic ashes to the regional geochemical balance: The 2008 eruption of Chaiten volcano, Southern Chile. Science of the Total Environment, 425, 75-88.

Ruxton, B.P., 1968. Measures of the degree of chemical weathering of rocks. The Journal of Geology, 76(5), 518-527.

Saylor, B.Z., Poling, J.M., Huff, W.D., 2005. Stratigraphic and chemical correlation of volcanic ash beds in the terminal Proterozoic Nama Group, Namibia. Geological Magazine, 142(5), 519-538.

Schroeder, P.A., Nagasawa, K., 1992. A multiple reaction mechanism (MRM) model for illitization during burial diagenesis, *in* Clay Minerals and Their Natural Resources. 29th International Geological Congress Workshop WB-1, Kyoto, Japan, 88 pp.

Schroeder, P.A., Shiflet, J., 2000. Ti-bearing phases in the Huber Formation, an East Georgia kaolin deposit. Clays and Clay Minerals, 48(2), 151-158.

Schulz, H., Wirth, R., Schreiber, A., 2016. Nano-crystal formation of TiO_2 polymorphs brookite and anatase due to organic—inorganic rock–fluid interactions. Journal of Sedimentary Research, 86(2), 59-72.

Senkayi, A.L., Dixon, J.B., Hossner, L.R., Abder-Ruhman, M., Fanning, D.S., 1984. Mineralogy and genetic relationships of tonstein, bentonite, and lignitic strata in the Eocene Yegua Formation of east-central Texas. Clays and Clay Minerals,

32(4), 259-271.

Shen, J., 2014. Volcanic Effects to Marine Environments and Organisms Across the Permian-Triassic Transition in South China, Ph.D. dissertation, China University of Geosciences, Wuhan, China.

Shen, J., Algeo, T.J., Feng, Q., Zhou, L., Feng, L., Zhang, N., Huang, J., 2013. Volcanically induced environmental change at the Permian-Triassic boundary (Xiakou, Hubei Province, South China): related to West Siberian coal-field methane releases? Journal of Asian Earth Sciences, 75, 95-109.

Shen, M.L., Dai, S.F., Graham, I.T., Nechaev, V.P., French, D., Zhao, F.H., Shao, L.Y., Liu, S.D., Zuo, J.P., Zhao, J.T., Chen, K., Xie, X.H., 2021. Mineralogical and geochemical characteristics of altered volcanic ashes tonsteins and K-bentonites) from the latest Permian coal-bearing strata of western Guizhou Province, southwestern China. International Journal of Coal Geology, 237, 103707.

Skrabal, S.A., 2006. Dissolved titanium distributions in the Mid-Atlantic Bight. Marine Chemistry, 102(3-4), 218-229.

Somelar, P., Kirsimaee, K., Srodon, J., Cuadros, J., Gorniak, K., Bahranowski, K., Labrincha, J., 2009. Mixed-layer illite-smectite in the Kinnekulle K-bentonite, northern Baltic Basin. Clay Minerals, 44(4), 455-468.

Sucha, V., Kraus, I., Gerthofferova, H., Petes, J., Serekova, M., 1993. Smectite to illite conversion in bentonites and shales of the East Slovak Basin. Clay Minerals, 28(2), 243-253.

Tan, M., Zhao, B., Zhou, B., Zhang, X., 2016. Geochemical characteristics and genesis of T/P boundary clay and event clay in Da-fang aera, Guizhou Province. Geological Bulletin of China, 35(6), 979-988.

Taylor, S.R., McLennan, S.M., 1985. The Continental Crust: Its Composition and Evolution, Blackwell, Oxford, 312 pp.

Tuğrul, A., 2004. The effect of weathering on pore geometry and compressive strength of selected rock types from Turkey. Engineering Geology, 75(3-4), 215-227.

Uddin, M.K., 2017. A review on the adsorption of heavy metals by clay minerals, with special focus on the past decade. Chemical Engineering Journal, 308, 438-

462.

Wang L., Zhang J., Chen J., Zhang Y., Chen X., Zhu Z., Liu J., Hu Y., 2015. Characteristics of Upper Ordovician potassic porphyry in Anji, Zhejiang Province. Journal of Stratigraphy, 39(2), 155-168.

Wang, X., Wang, H., 2021. Structural analysis of interstratified illite-smectite by the Rietveld method. Crystals, 11(3), 244, 15 pp.

Wang, Z., 1998. Sedimentary facies and sequence stratigraphy of Permian in Daxiakou, Xingshan, Hubei Province. Journal of Oil and Gas Technology (03), 4-10.

Wang Z., Zhou H., Wang T., Jing X., Zhang Y., 2015. Ordovician volcanic activity records in the southwest margin of Ordos Basin: geochemical and zircon chronology information from Pingliang Formation potassic porphyry in Shaan-Gan area. Acta Petrologica Sinica (9), 22.

Weaver, C.E., Pollard, L.D., 1973. The Chemistry of Clay Minerals. Elsevier, Amsterdam, 213 pp.

Wilson, M.J., Shaldybin, M.V., Wilson, L., 2016a. Clay mineralogy and unconventional hydrocarbon shale reservoirs in the USA. I. Occurrence and interpretation of mixed-layer R3 ordered illite/smectite. Earth-Science Reviews, 158, 31-50.

Wilson, M.J., Wilson, L., Shaldybin, M.V., 2016b. Clay mineralogy and unconventional hydrocarbon shale reservoirs in the USA. II. Implications of predominantly illitic clays on the physico-chemical properties of shales. Earth-Science Reviews, 158, 1-8.

Xiao, Y., 2017. Study on Fine Structure and Formation of Mixed-Layer Illite/Smectite Clays by Short-Wave Infrared Spectroscopy–A Case Study of Clay Rock near the P-T Boundary in South China. M.S. Thesis. China University of Geosciences-Wuhan, 44 pp. (in Chinese with English abstract).

Xu, G., Deconinck, J.F., Feng, Q., Baudin, F., Pellenard, P., Shen, J., Bruneau, L., 2017. Clay mineralogical characteristics at the Permian–Triassic Shangsi section and their paleoenvironmental and/or paleoclimatic significance. Palaeogeography, Palaeoclimatology, Palaeoecology, 474, 152-163.

Yang, S., Hu, W., Wang, X., Jiang, B., Yao, S., Sun, F., Huang, Z., Zhu, F., 2019. Duration, evolution, and implications of volcanic activity across the Ordovician–Silurian transition in the Lower Yangtze region, South China. Earth and Planetary Science Letters, 518, 13-25.

Yang, S., Hu, W., Fan, J., Deng, Y., 2022. New geochemical identification fingerprints of volcanism during the Ordovician-Silurian transition and its implications for biological and environmental evolution. Earth-Science Reviews, 228, 104016.

Yu, J., Broutin, J., Chen, Z.Q., Shi, X., Li, H., Chu, D., Huang, Q., 2015. Vegetation changeover across the Permian–Triassic Boundary in Southwest China: Extinction, survival, recovery and palaeoclimate: A critical review. Earth-Science Reviews, 149, 203-224.

Yuan, P., Liu, H., Liu, D., Tan, D., Yan, W., He, H., 2013. Role of the interlayer space of montmorillonite in hydrocarbon generation: An experimental study based on high temperature–pressure pyrolysis. Applied Clay Science, 75-76, 82-91.

Zanetta, P., Rao Manga, V., Chang, Y., Ramprasad, T., Weber, J., Beckett, J.R., Zega, T.J., 2023. Atomic-scale characterization of the oxidation state of Ti in meteoritic hibonite: Implications for early solar system thermodynamics. American Mineralogist, 108(5), 881-902.

Zhang, J.M., Zhu, M.Y., Yang, A.H., Li, G.X., Yang, J.H., Heubeck, C., 2004. Stratigraphic implications of Sinian-Early Cambrian volcanic ash beds on the Yangtze Platform. Progress in Natural Science–Materials International, 47(2), 92-97.

Zhang, S.X., Zhao, L., Tong, J., Yang, H., 2007. Study on clay rocks near the Permian-Triassic boundary in Daxiakou, Xingshan, Hubei Province. Journal of Mineralogy and Petrology, 27(3), 7.

Zhou, D., Abdel-Fattah, A.I., Keller, A.A., 2012. Clay particles destabilize engineered nanoparticles in aqueous environments. Environmental Science & Technology, 46(14), 7520-7526.

Zhou, M., Wan, B., Zhou, L., Yang, E., Yang, L., Luo, T., 2021. Origin of K-bentonite in the Doushantuo cap dolostones from South China and its potential link with the sedimentary model of the Marinoan cap dolostones. Precambrian Research,

366, 106416.

Zhou, Y., Bohor, B.F., Ren, Y., 2000. Trace element geochemistry of altered volcanic ash layers (tonsteins) in Late Permian coal-bearing formations of eastern Yunnan and western Guizhou Provinces, China. International Journal of Coal Geology, 44(3-4), 305-324.

Zhu, X., Zhang, B., Ma, G., Pan, Z., Hu, Z., Zhang, B., 2022. Mineralization of ion-adsorption type rare earth deposits in Western Yunnan, China. Ore Geology Reviews, 148, 104984.

Table 1. Global bentonite bearing sections from different depositional environment

Sedimentary facies	Location	Ash layers	Sources
Deep marine	Dongpan	9	Shen, 2014
	Xinmin	19	
	Chaotian	2	
	Shangsi	2	He et al., 2014
	Rencunping	3	
	Changqiao	4	
	Caicun	8	Liao et al., 2016
	Niushan	8	
	Duanshan	6	Gong et al., 2018
	Pingliang	10	Wang et al., 2015
	Argentine Precordillera	10	Huff et al., 1998
	China	4	Zhou et al., 2021
Shallow marine	Famatina	4	Astini et al., 2007
	Lunshan	16	Yang et al., 2019
	Xinqiao,Anji	6	Wang et al., 2015
	Grimstorp Series	14	
	Kinnekulle Bentonite.	12	Kiipli et al., 2014
	Sinsen and Grefsen Series.	55	
	Gotland,Sweden	12	Batchelor and Jeppson, 1999
	Norway and	28	Batchelor, 2014
	Sweden	16	
	Xiakou	7	Zhang et al., 2007
	Liulong	7	Tan et al., 2016
	Meishan	2	He et al., 2014
	Zhongzhai	2	Hong et al., 2017
	Pengda	7	Xiao, 2017
	Yanlou	6	
	Xiakou	6	-
	Reşadiye	23	Kadir et al., 2021
	Zhaolaoyu	7	Cheng et al., 2012
	Huanglianba	4	Zhang et al., 2004
paludal	Guizhou	12	Shen et al., 2021
	Zhejue	2	Hong et al., 2017
	Chahe	4	Gong et al., 2018
	Tucheng	3	Hong et al., 2019
	Jinzhong	5	Xiao, 2017
lacustrine	Chahe	3	Gong, 2018
	Jiucaichong	1	Hong et al., 2019
	Chahe	2	Zhang et al.,2004

	ŞIle	18	Ece. et al., 2003
	ŞIle	11	
	Chile	4	Ruggieri et al., 2012

Table 2. Fitting results for clay fraction of altered volcanic ash sample after EG treatment

Sample	Phase	R	W%	N	W_a(I %)	$W_b/(W_b+W_c)$
L255	ISS	1	53%	5.14	77	0.97
	ISS	1	47%	6.22	62	0.51
L260	ISS	1	63%	5.64	75	1
	ISS	1	37%	7.96	62	0.37
L264	ISS	1	70%	7.96	76	0.92
	ISS	1	26%	9.41	68	0.47
	Illite	-	4%	23.62	-	-
L266	ISS	1	63%	7.38	78	0.85
	ISS	1	36%	5.64	63	0.43
	Kaolinite	-	1%	10.36	-	-
L271	ISS	1	76%	7.38	78	0.85
	ISS	1	21%	5.64	63	0.34
	Kaolinite	-	3%	10.36	-	-
L277	ISS	1	100%	9.41	76	0.76

Notes: R is Reichweite, W% is the weight percent of this phase, N is the average CSDS, W_a is the percentage of illite layer in the I-S, W_b and W_c is the occurrence probability of smectite layer with two ethylene glycol complexes and one ethylene glycol complex respectively.

Table 3. Major-element compositions of the Xiakou altered volcanic ash (wt%)

Sample	SiO_2	TiO_2	Al_2O_3	Fe_2O_3	MnO	MgO	CaO	Na_2O	K_2O	P_2O_5	LOI	SiO_2/ Al_2O_3	CIA	CIW
L277	52.30	0.36	24.64	2.56	0.00	3.43	1.27	0.07	6.07	0.03	7.31	3.60	78	99
L271	53.34	0.50	25.49	1.33	0.00	3.58	1.31	0.08	6.18	0.04	7.11	3.55	79	99
L266	48.22	0.48	21.83	4.93	0.01	3.13	1.11	0.14	5.38	0.06	11.92	3.75	78	98
L264	51.14	0.42	20.44	4.90	0.02	3.25	1.31	0.42	5.32	0.05	10.11	4.25	74	94
L260	49.37	0.36	23.26	3.22	0.01	3.53	1.90	0.05	5.76	0.06	8.16	3.60	78	99
L255	54.34	0.42	22.94	3.11	0.00	3.69	0.91	0.17	5.57	0.11	7.95	4.02	78	98
MS-A-25*	50.88	0.45	26.36	3.07	0.00	3.31	0.94	0.07	5.23	0.10	9.91	3.28	82	99
MS-A-28*	57.85	0.74	16.45	5.05	0.03	2.54	4.41	0.19	4.46	0.06	8.49	5.97	75	96

Note: The Major-element composition of K-bentonite of Meishan section from He et al. (2014), All Fe as Fe_2O_3; LOI is loss on ignition

Table 4. Concentrations of trace elements and REEs of the Xiakou altered volcanic ash (ppm)

Sample	La	Ce	Pr	Nd	Sm	Eu	Gd	Tb	Dy	Ho	Er	Tm	Yb	Lu	Hf	ΣREE	ΣLREE	ΣHREE	ΣLREE/ΣHREE
L277	26.82	73.40	8.80	32.68	8.14	1.38	7.63	1.36	7.59	1.41	3.68	0.48	2.77	0.38	15.28	191.81	151.23	40.59	3.73
L271	37.13	96.60	11.16	40.01	8.31	1.40	7.14	1.31	7.20	1.37	3.60	0.46	2.65	0.37	16.42	235.14	194.61	40.54	4.80
L266	28.02	77.96	9.35	34.56	6.36	0.93	5.34	1.11	6.55	1.33	3.58	0.50	2.96	0.41	13.37	192.33	157.17	35.15	4.47
L264	13.61	24.07	2.62	9.26	2.00	0.43	1.96	0.44	2.73	0.58	1.77	0.28	1.81	0.28	7.83	69.67	52.00	17.67	2.94
L260	56.10	129.39	13.60	43.64	6.36	0.70	4.78	0.99	6.53	1.32	3.88	0.54	3.15	0.44	12.63	284.03	249.78	34.25	7.29
L255	53.23	106.41	11.60	39.39	6.60	0.75	4.53	0.74	4.58	0.86	2.26	0.30	1.84	0.26	8.12	241.48	217.99	23.50	9.28

This is the peer-reviewed, final accepted version for American Mineralogist, published by the Mineralogical Society of America.
The published version is subject to change. Cite as Authors (Year) Title. American Mineralogist, in press.
DOI: https://doi.org/10.2138/am-2023-9125. http://www.minsocam.org/

Sample	Li	Be	Sc	V	Cr	Co	Ni	Cu	Zn	Ga	Rb	Sr	Y	Zr	Nb	Sn	Cs	Ba	Ta	Tl	Pb	Th	U
L277	74.8	2.09	12.0	6.25	1.51	1.41	2.18	9.61	55.71	27.71	125.87	91.21	40.30	274	15.90	8.15	11.96	40.02	2.28	0.19	26.47	43.70	2.62
L271	86.3	3.03	15.8	16.5	5.16	1.58	6.03	19.12	98.19	27.85	126.72	114.77	39.48	297	18.02	8.70	11.28	65.35	2.68	0.09	15.22	53.26	3.05
L266	58.7	2.65	17.2	32.6	10.2	4.84	15.23	22.54	28.13	21.61	110.08	196.96	36.00	207	14.57	7.29	13.59	89.43	2.25	1.48	21.64	51.47	3.77
L264	71.6	2.74	7.98	60.7	26.8	4.77	15.81	20.36	26.73	22.19	125.21	176.43	16.13	455	15.62	9.48	13.51	189.31	3.59	1.84	30.81	48.83	2.75
L260	74.9	2.31	13.1	10.5	3.38	1.73	10.62	11.99	21.66	25.39	100.86	367.06	35.68	191	14.64	8.97	11.81	159.44	2.20	1.12	56.92	52.35	5.00
L255	93.7	1.46	8.72	48.8	11.9	1.89	5.57	13.17	29.08	25.75	115.40	197.46	20.98	602	11.63	7.14	10.66	158.00	1.74	1.15	53.06	36.85	5.18

Table 5. The occurrence of authigenic titanium oxides in different sedimentary environments

Environment	Lithology	Phase	Occurrence of titanium minerals	Source
Continental shelf and slope-basin	shale	anatase, brookite	brookite crystallized invariably along cleavages of detrital biotite and anatase intergrowed with bitumen	Liu et al., 2019
Swamp	tonstein	anatase	anatase replacing glass shards, or as individual anatase crystals	Ruppert and Moore, 1993
Swamp	tonstein	anatase	anatase in the interspace of kaolinite, or as discrete anatase aggregates	Dai et al., 2014
None-marine	kaolin deposit	anatase	anatase as fine-grained and rounded crystals in pocket within kaolinite	Hassan, 2014
Shallow marine	sandstone	anatase, brookite	pseudomorphs after Fe-Ti-oxides	Morad, 1988
Shore	sandstone	brookite	brookite as boxworks between other detrital minerals, or small plate in leucoxene or attaching to altered ilmenite	Sun and Allen, 1957
Shallow marine	sandstone shale carbonate	leucoxene	crystallized leucoxene crystals	Morad and Aldahan, 1982
Shallow marine	claystone	anatase, rutile	as needle-like crystals (weak metamorphism)	Allo, 2004
Altered dacite	dacite	anatase	anatase as connected platy grains paralleling to the mica layers, or in the altered ilmenite	Papoulis, 2009

This is the peer-reviewed, final accepted version for American Mineralogist, published by the Mineralogical Society of America.
The published version is subject to change. Cite as Authors (Year) Title. American Mineralogist, in press.
DOI: https://doi.org/10.2138/am-2023-9125. http://www.minsocam.org/

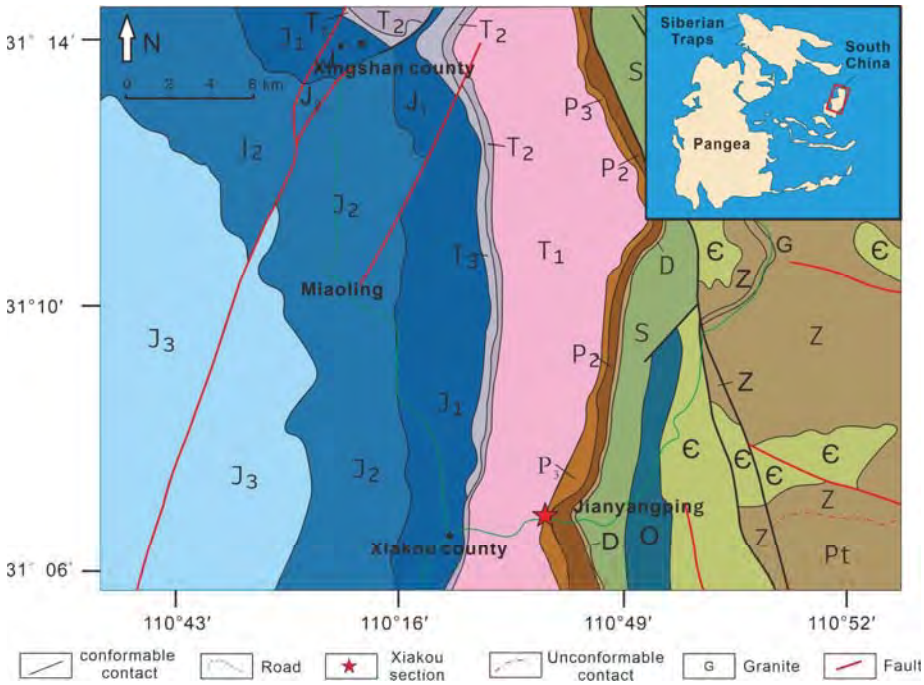

Figure 1. Geological map of the Xiakou Area depicting location, lithology, and structural features. The red star represents the study area. The inset shows global distribution of landmasses during the Late Permian.

Figure 2. View of the full Xiakou section. The orange line and the corresponding marks show the positions of the sampled altered volcanic ash beds.

This is the peer-reviewed, final accepted version for American Mineralogist, published by the Mineralogical Society of America.
The published version is subject to change. Cite as Authors (Year) Title. American Mineralogist, in press.
DOI: https://doi.org/10.2138/am-2023-9125. http://www.minsocam.org/

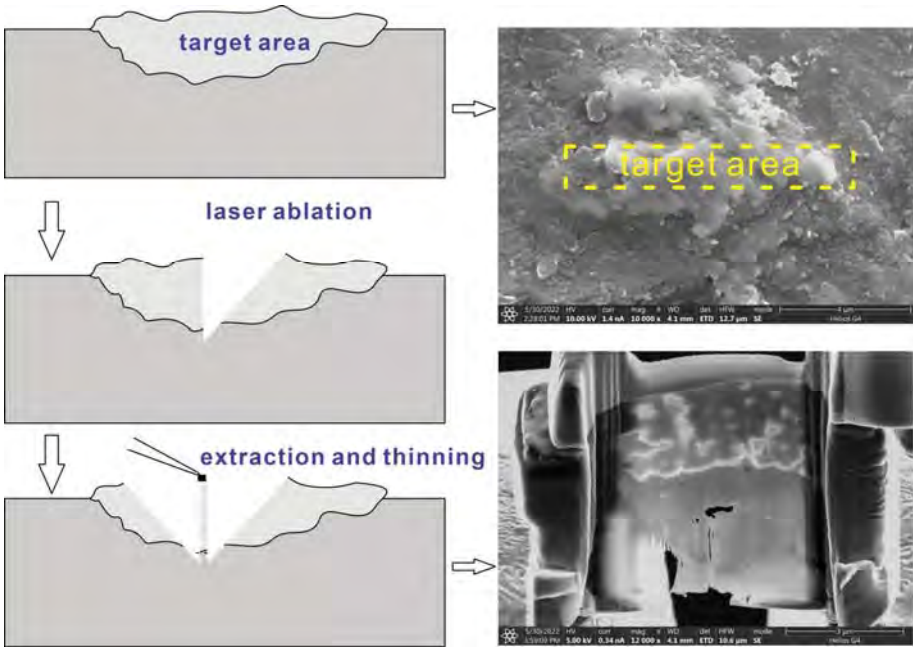

Figure 3. Schematic steps of FIB thinning treatment and the corresponding SEM images.

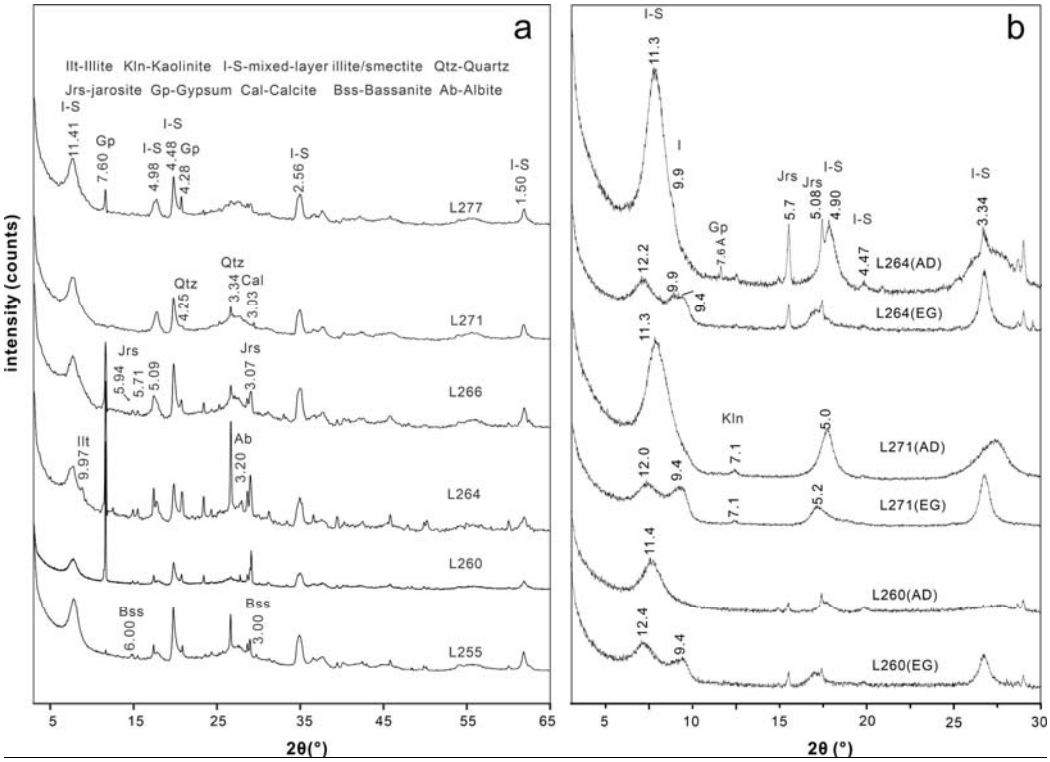

Figure 4. XRD patterns for representative bulk samples (a) and clay fractions (b) of Xiakou altered volcanic ash. All mineral names are indicated in abbreviated form, abbreviations for corresponding minerals can be found in the upper part of panel 'a'.

This is the peer-reviewed, final accepted version for American Mineralogist, published by the Mineralogical Society of America.
The published version is subject to change. Cite as Authors (Year) Title. American Mineralogist, in press.
DOI: https://doi.org/10.2138/am-2023-9125. http://www.minsocam.org/

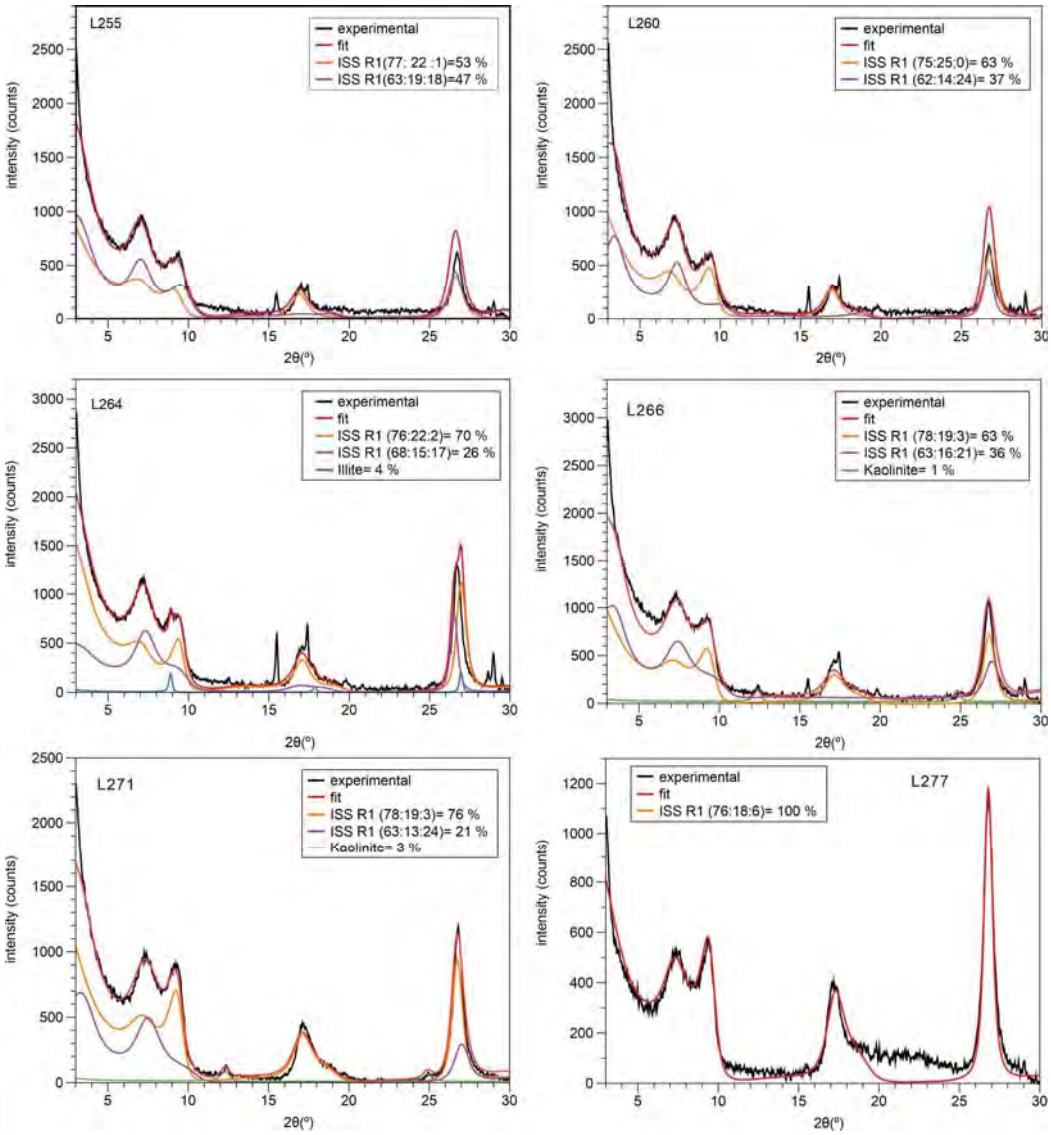

Figure 5. Fitting patterns of clay fractions of the Xiakou altered volcanic ash samples (EG saturation).

This is the peer-reviewed, final accepted version for American Mineralogist, published by the Mineralogical Society of America.
The published version is subject to change. Cite as Authors (Year) Title. American Mineralogist, in press.
DOI: https://doi.org/10.2138/am-2023-9125. http://www.minsocam.org/

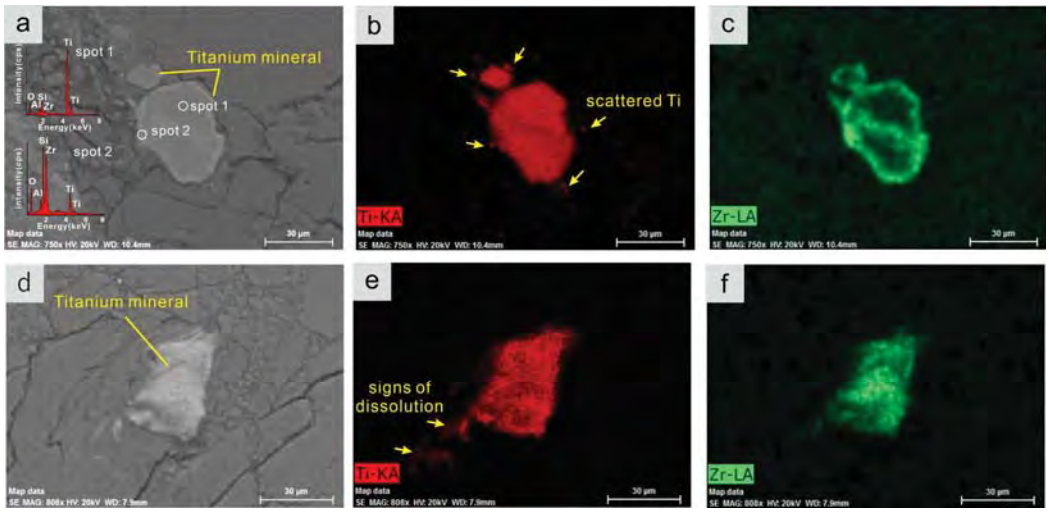

Figure 6. SEM images showing the morphology and chemical composition of the Ti-bearing minerals in altered volcanic ash. (a)-(c) TiO_2 aggregates with Zr concentrated along edges. (b) Altered srilankite exhibiting a spatial relationship to scattered titanium minerals. (d)-(f) TiO_2 aggregates composed of Ti and Zr.

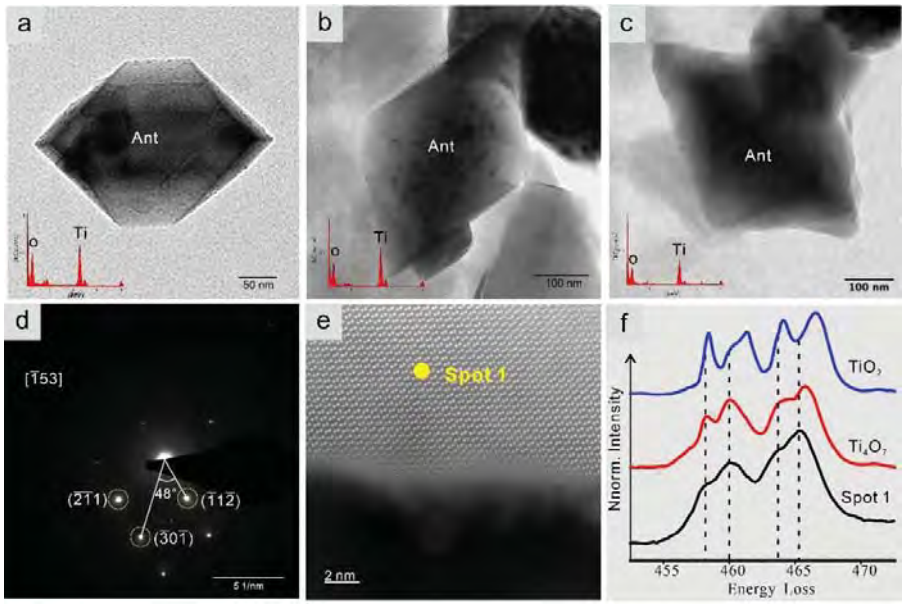

Figure 7. HRTEM images of anatase with EDS profile for the Xiakou altered volcanic ash. (a)-(c) Nanoscale anatase with bipyramidal crystal morphologies. (d) SAED pattern of anatase crystal (c). (e) and (f) EELS analysis of the edge of a Ti particle and comparation between the EELS spectra of spot 1 and Ti-oxides in various oxidation states (Zanetta et al., 2023).

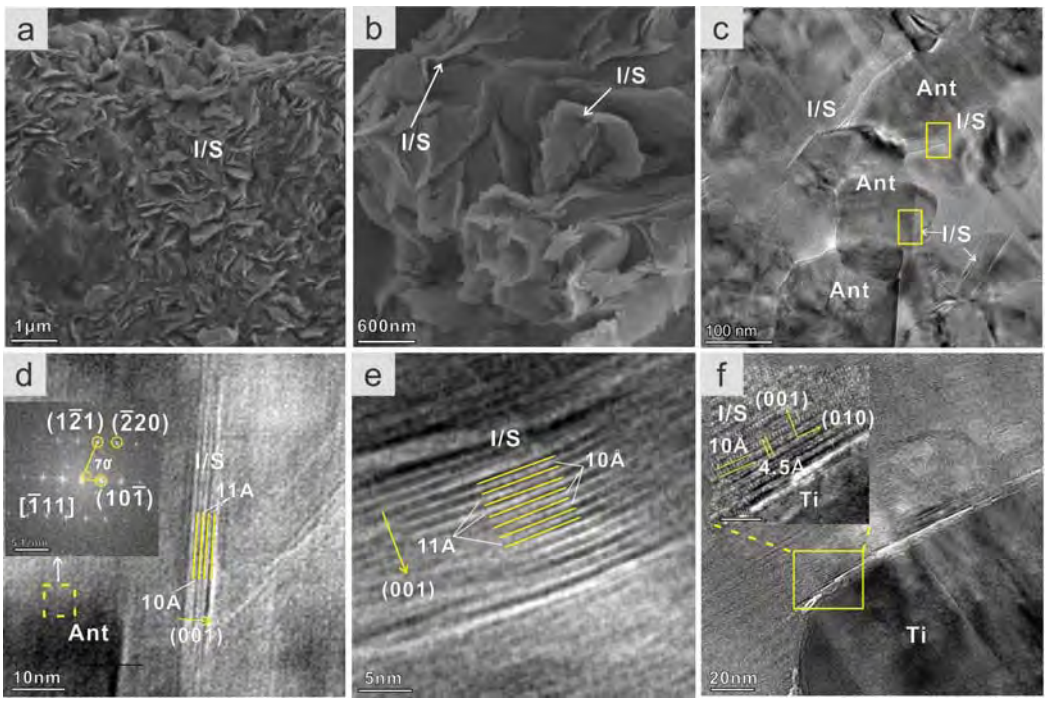

Figure 8. SEM images of I-S within the altered volcanic ash sample (a-b) and the HRTEM images of I-S and anatase (c-f). The I-S clays in the Xiakou altered volcanic ash (a-b) have a platy habit and curved edges with thicknesses of 15-25 nm, and they are closely associated with anatase (c-f).

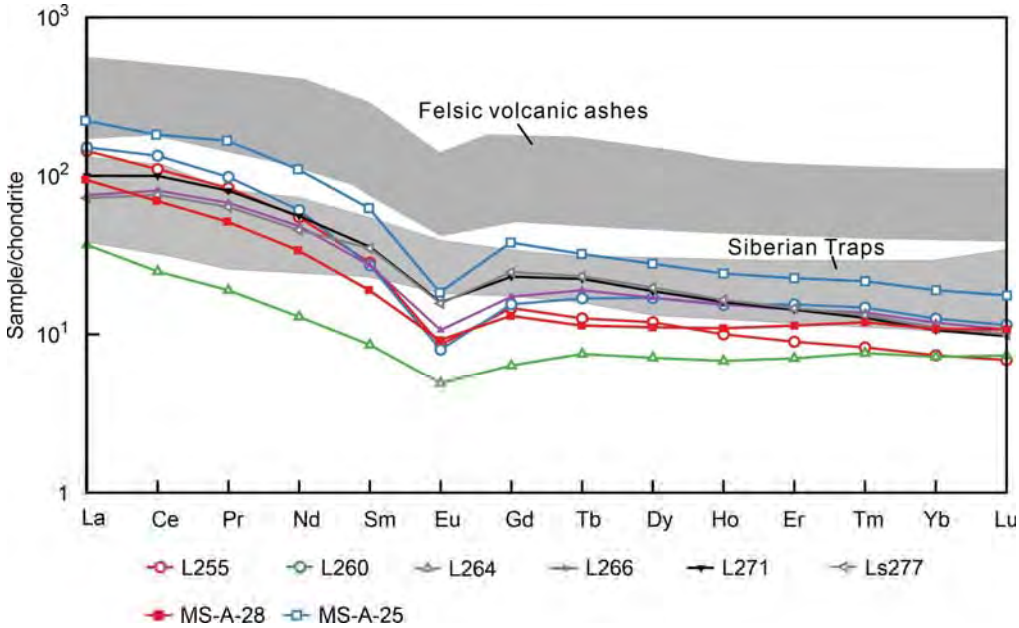

Figure 9. REE distributions of Xiakou bulk altered volcanic ash samples normalized to chondrite composition (Carbonaceous Ivuna (CCI) chondrite from Taylor and McLennan (1985)); REE patterns of felsic volcanic ash beds at Meishan are from He et al. (2014), REE patterns for the Siberian Traps are from Malitch et al. (2010).

This is the peer-reviewed, final accepted version for American Mineralogist, published by the Mineralogical Society of America.
The published version is subject to change. Cite as Authors (Year) Title. American Mineralogist, in press.
DOI: https://doi.org/10.2138/am-2023-9125. http://www.minsocam.org/

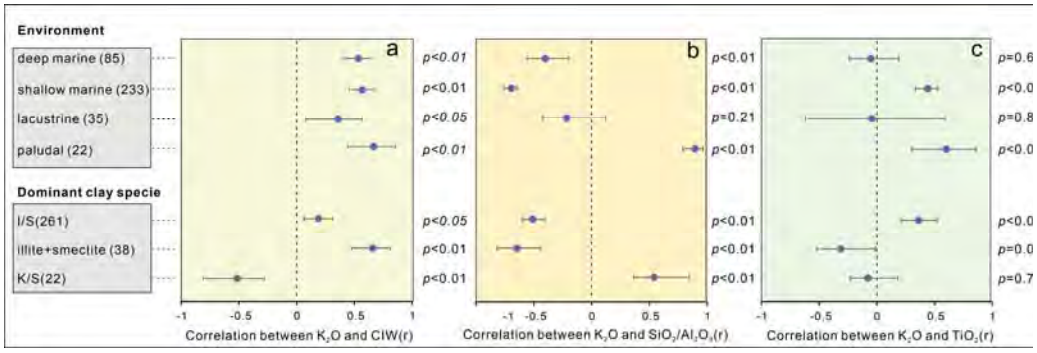

Figure 10. Forest plots of the correlations between K_2O content and weathering indexes (a-b), and between K_2O and TiO_2 contents (c). The meta-analysis data were grouped into two types according to depositional environment and dominant clay species. Data points represent Pearson's *r*, and the bars represent the 95% confidence interval.

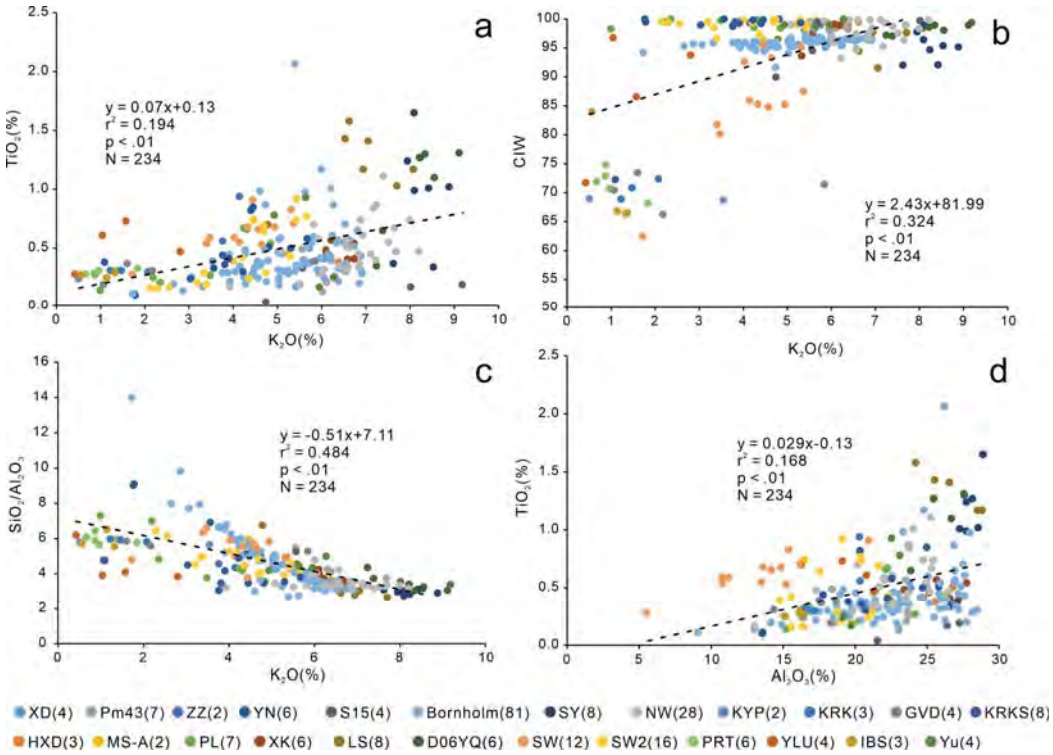

Figure 11. Scatterplots of weathering indices (CIW and R) and TiO_2 content versus K_2O content of bentonite (a-c), and of TiO_2 content versus Al_2O_3 content in (K-)bentonite (d). All data shown in this figure are for (K-)bentonites deposited in shallow-marine settings. The legend at bottom indicates section names and number of (K-)bentonites analyzed in each section.

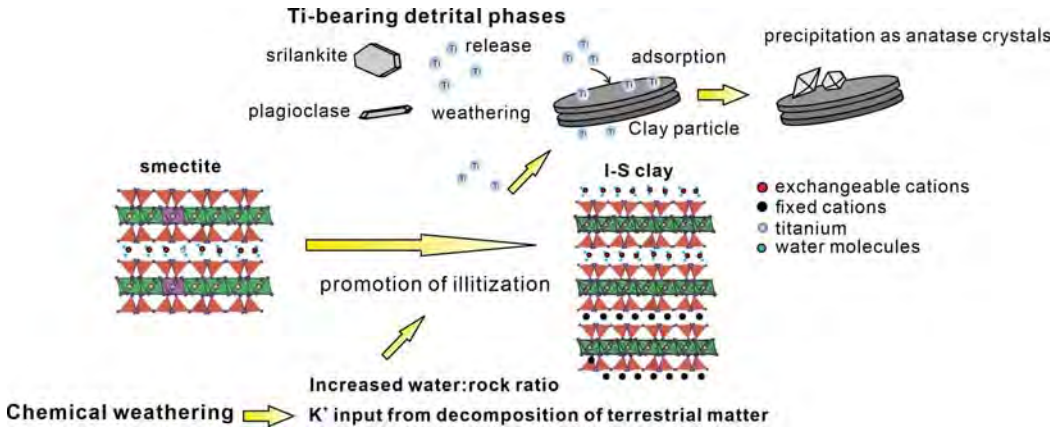

Figure 12. Clay particle association and the formation path of authigenic anatase. Following the deposition of volcanic ash, the glass fraction undergoes transformation into smectitic minerals, which then further evolve into I-S clays. The illitization process, along with the alteration of srilankite and plagioclase, represents a titanium (Ti) source for the formation of anatase. The Ti is subsequently adsorbed by the surface of I-S clay particles due to its high specific surface area, which results in precipitation of anatase crystals that are closely associated with I-S.